AMERICAN SOCIETY FOR MICROBIOLOGY | mBio®

RESEARCH ARTICLE

Identification and Characterization of the Novel Subunit CcoM in the cbb_3-Cytochrome *c* Oxidase from *Pseudomonas stutzeri* ZoBell

Martin Kohlstaedt,[a] Sabine Buschmann,[a] Hao Xie,[a] Anja Resemann,[b] Eberhard Warkentin,[a] Julian D. Langer,[a] Hartmut Michel[a]

Department of Molecular Membrane Biology, Max Planck Institute of Biophysics, Frankfurt am Main, Germany[a]; Bruker Daltonik GmbH, Bremen, Germany[b]

ABSTRACT **Cytochrome *c* oxidases (C*c*Os), members of the heme-copper containing oxidase (HCO) superfamily, are the terminal enzymes of aerobic respiratory chains. The cbb_3-type cytochrome *c* oxidases (cbb_3-C*c*O) form the C-family and have only the central catalytic subunit in common with the A- and B-family HCOs. In *Pseudomonas stutzeri*, two cbb_3 operons are organized in a tandem repeat. The atomic structure of the first cbb_3 isoform (Cbb_3-1) was determined at 3.2 Å resolution in 2010 (S. Buschmann, E. Warkentin, H. Xie, J. D. Langer, U. Ermler, and H. Michel, Science 329:327–330, 2010, http://dx.doi.org/10.1126/science.1187303). Unexpectedly, the electron density map of Cbb_3-1 revealed the presence of an additional transmembrane helix (TMH) which could not be assigned to any known protein. We now identified this TMH as the previously uncharacterized protein PstZoBell_05036, using a customized matrix-assisted laser desorption ionization (MALDI)–tandem mass spectrometry setup. The amino acid sequence matches the electron density of the unassigned TMH. Consequently, the protein was renamed CcoM. In order to identify the function of this new subunit in the cbb_3 complex, we generated and analyzed a CcoM knockout strain. The results of the biochemical and biophysical characterization indicate that CcoM may be involved in C*c*O complex assembly or stabilization. In addition, we found that CcoM plays a role in anaerobic respiration, as the ΔCcoM strain displayed altered growth rates under anaerobic denitrifying conditions.**

IMPORTANCE **The respiratory chain has recently moved into the focus for drug development against prokaryotic human pathogens, in particular, for multiresistant strains (P. Murima, J. D. McKinney, and K. Pethe, Chem Biol 21:1423–1432, 2014, http://dx.doi.org/10.1016/j.chembiol.2014.08.020). cbb_3-C*c*O is an essential enzyme for many different pathogenic bacterial species, e.g., *Helicobacter pylori*, *Vibrio cholerae*, and *Pseudomonas aeruginosa*, and represents a promising drug target. In order to develop compounds targeting these proteins, a detailed understanding of the molecular architecture and function is required. Here we identified and characterized a novel subunit, CcoM, in the cbb_3-C*c*O complex and thereby completed the crystal structure of the Cbb_3 oxidase from *Pseudomonas stutzeri*, a bacterium closely related to the human pathogen *Pseudomonas aeruginosa*.**

Received 9 December 2015 **Accepted** 21 December 2015 **Published** 26 January 2016

Citation Kohlstaedt M, Buschmann S, Xie H, Resemann A, Warkentin E, Langer JD, Michel H. 2016. Identification and characterization of the novel subunit CcoM in the cbb_3-cytochrome *c* oxidase from *Pseudomonas stutzeri* ZoBell. mBio 7(1):e01921-15. doi:10.1128/mBio.01921-15.

Invited Editor Fevzi Daldal, University of Pennsylvania **Editor** Howard A. Shuman, University of Chicago

Address correspondence to Julian D. Langer, julian.langer@biophys.mpg.de, or Hartmut Michel, hartmut.michel@biophys.mpg.de.

In recent years, the central bacterial metabolic enzymes have become prime targets for the development of new antibiotic drugs (1). The heme-copper containing oxidase (HCO) superfamily comprises the terminal enzymes of the aerobic respiratory chain as well as the nitric oxide reductases (NOR) which are involved in anaerobic respiration. Terminal oxidases are present in the respiratory chains of eukaryotes and many prokaryotes and thus represent tempting candidates for drug development. They catalyze the four-electron reduction of molecular oxygen to water and couple this exergonic reaction to transmembrane proton pumping, thus contributing to the generation of the electrochemical proton gradient across the membrane.

HCOs can be classified into three major families: A, B, and C (2). To date, at least one crystal structure has been published for each family (3–6). The C-family consists only of the cbb_3-type cytochrome *c* oxidases (cbb_3-C*c*Os) which are predominantly found in bacteria (7). In the genus *Pseudomonas*, the genes encoding the two isoforms of cbb_3-C*c*Os (Cbb_3-1 and Cbb_3-2) are organized as a tandem repeat (8, 9).

In *Pseudomonas stutzeri*, only the second cbb_3 operon contains a fourth gene (*ccoQ*) in addition to the *ccoN*, *ccoO*, and *ccoP* (*ccoNOP*) genes (6, 10). The crystal structure of Cbb_3-1 from *P. stutzeri* was determined at a resolution of 3.2 Å in 2010. Surprisingly, besides the known CcoNOP subunits, the electron density map revealed the presence of an additional fourth subunit consisting of a single transmembrane helix (TMH) (6). It is located in close proximity to helices VIII, IX, and XI of the catalytic subunit CcoN. Prior to this study, neither proteomic nor genomic information was available for this subunit.

In this work, we set out to identify and characterize this as-yet-undescribed subunit of cbb_3-C*c*O whose gene is located outside the main cbb_3 operon. We purified and subsequently sequenced the polypeptide using matrix-assisted laser desorption ionization time-of-flight tandem mass spectrometry (MALDI-TOF MS/MS) and propose to rename PstZoBell_05036 CcoM. To determine the physiological role of CcoM in the cbb_3 complex, we created a deletion strain for this gene and monitored its growth rates under

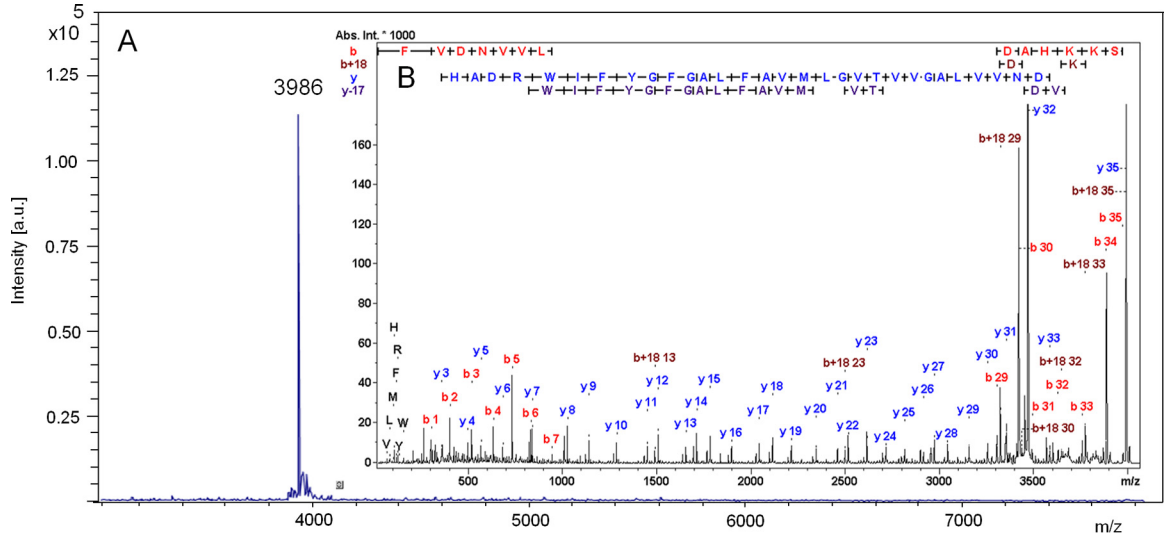

FIG 1 MALDI-TOF MS measurements. (A) MALDI-TOF MS measurement of the 90% (vol/vol) acetonitrile elution fraction of c4-ZipTiped purified Cbb_3-1 oxidase with a peak at 3,986 Da (monoisotopic mass). a.u., arbitrary units. (B) MALDI-TOF MS/MS spectrum of the precursor detected with MALDI-TOF MS with *m/z* 3,986. A Mascot database search identified the sequence MFVDNVVLAGVVTVGLMVAFLAGFGYFIWRDAHKKS with a modification of 28 Da at the N-terminus which was assigned to formylation. Abs. Int., absolute intensity.

different conditions. Furthermore, we compared the purified Cbb_3-1–ΔCcoM variant and the wild-type Cbb_3-1 using ultraviolet-visible light (UV-vis) spectroscopy, differential scanning calorimetry (DSC), and oxygen reductase activity measurements.

RESULTS

Identification of an uncharacterized C*c*O subunit. On the basis of the X-ray crystallographic electron density, we estimated that the unidentified subunit consists of one TMH with an overall size of 30 to 45 amino acids. We thus purified the full C*c*O complex by column chromatography (11) and immobilized the proteins on a c4 solid-phase extraction column. Sequential elution using organic solvent allowed us to generate a fraction enriched in a polypeptide with a monoisotopic molecular mass of 3,986 Da (Fig. 1A). Since we were not able to annotate a matching protein in the *P. stutzeri* proteome, we performed tandem-MS measurements on a Bruker ultrafleXtreme MALDI-TOF mass spectrometer. The sequence tags derived from *de novo* sequencing matched the hypothetical PstZobell_05036 protein in an MS_BLAST search with a score of 134 (Fig. 1B). Upon matching the sequence to the MS/MS spectrum in BioTools, an N-terminal mass shift of 28 Da was assigned and explained as N-terminal formylation, caused by the presence of a starting N-formylmethionine. The result was confirmed by a direct protein search of the NCBI Nr database using Mascot 2.4 with N-terminal formylation as a variable modification and a Mascot score of 352.

Fitting of the identified peptide into the unassigned TMH of Cbb_3-1. A BLAST search of the identified peptide was performed against the NCBI "draft genome of *P. stutzeri* ATCC 14405" database (12). One matching protein with the locus tag of PstZoBell_05036 consisting of 36 amino acids and described as "putative uncharacterized protein" was found. This protein is predicted to contain one membrane spanning an α-helix between Val7 and Trp29 as determined by the use of the TMHMM 2.0 server (http://www.cbs.dtu.dk/services/TMHMM/) (see Fig. S2 in the supplemental material). Residues 1 to 29 were fitted into the electron density map, and the model was subsequently refined. After refinement, the electron densities for the side chains were clearly improved. On the basis of these results, we renamed this protein CcoM. The residues located on the interface between CcoN and CcoM (e.g., T13, M17, F20, F24, and F27) match well with our structural template (Fig. 2A). Model building for the carboxy-terminal part of the peptide as well as the residues facing the exterior of the protein complex was not possible due to the absence of electron density. In summary, the majority of the amino acid side chains could be built into the electron density successfully, indicating that the observed TMH is correctly assigned to CcoM. On the basis of our determination of the placement into the crystal structure and due to the presence of a formyl group at the N-terminal methionine, CcoM has an N-terminus-out and C-terminus-in topology. In this orientation, the positively charged residues enriched in the C-terminal region of CcoM ($R_{30}DAH_{33}K_{34}K_{35}S\text{-}COO^-$; not visible in the crystal structure) reside in the cytosol, which is consistent with the "positive-inside" rule (13).

Interaction of CcoM with the *cbb*$_3$ complex. Subunit CcoM is still tightly bound to the Cbb_3-1 complex after four stringent purification steps and the crystallization process (11). This observation indicates a strong interaction between CcoM and the *cbb*$_3$-C*c*O complex. On the basis of our current structural model, we propose the idea of a ladder-like interaction between CcoM and helices VIII and IX of the catalytic subunit CcoN. The distances between these potentially interacting amino acids in each of the four *cbb*$_3$ monomers, present in the asymmetric unit of the crystal structure, are listed in Table S3 in the supplemental material. Figure 2B exemplarily represents the proposed interaction ladder of CcoN and CcoM based on chains A and N of Protein Data Bank [PDB] file 5DJQ, respectively. The phenylalanine residue (F20) of CcoM shows hydrophobic interactions with W284 of CcoN and a π-π interaction with F322. The edge-to-edge dis-

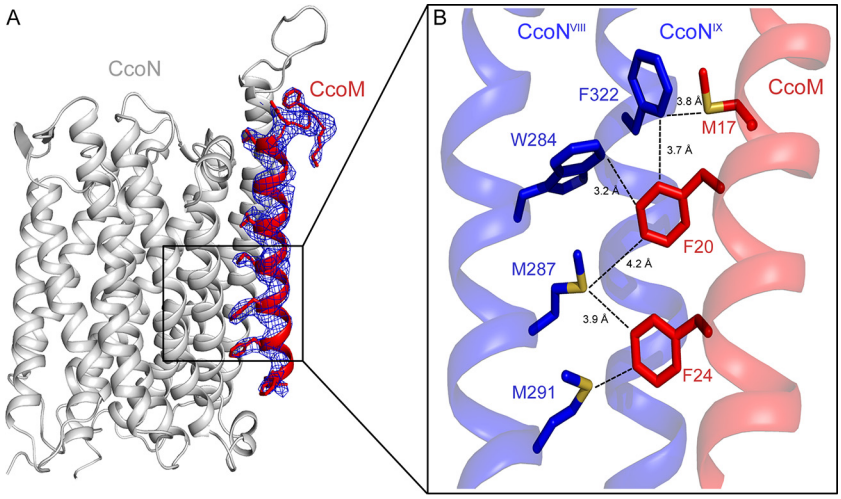

FIG 2 Interaction of CcoM and CcoN, exemplarily illustrated by chains N and A of PDB file 5DJQ, respectively. (A) Ribbon model of subunit CcoN (grey) and CcoM (red). The $2F_o$-F_c electron density map of CcoM is shown in blue at a level of 1.5 σ. CcoM residues matching the electron density are indicated as sticks (M1, F2, D4, V6, T13, M17, F20, F24, and F27). (B) Closeup of the proposed ladder-like interaction between helices VIII and IX of CcoN (blue) and CcoM (red). Sulfur-aromatic interactions ($M17^M$-$F322^N$, $F20^M$-$M287^N$, $F24^M$-$M287^N$, and $F24^M$-$M291^N$) and aromatic-aromatic interactions ($F20^M$-$W284^N$ and $F20^M$-$F322^N$) mainly contribute to the binding of CcoM to CcoN. The amino acids involved in interactions are shown as sticks, and their edge-to-edge distances are indicated. Sulfur atoms are shown in yellow.

tances between these residue pairs are 3.2 Å (F20-W284) and 3.7 Å (F20-F322), which corresponds to an optimal distance for a parallel sandwich arrangement of Phe-Phe pairs at 3.5 Å (14). In addition to the π-π interactions, we observed multiple sulfur-π interactions, including $M17^M$-$F322^N$, $F20^M$-$M287^N$, $F24^M$-$M287^N$, and $F24^M$-$M291^N$. The edge-to-edge distances of these interactions range from 3.8 to 4.2 Å and are comparable to the favorable distances of 3.6 and 5.5 Å for sulfur-π interactions (15). Furthermore, a Trp residue (W29) is present at the C-terminal end of the TMH in CcoM and is putatively oriented toward the lipid bilayer. Trp residues at the termini of transmembrane helices often interact with lipid headgroups and contribute to the stabilization of the position of the TMH in the lipid bilayer (16).

Analysis of CcoM. In *P. stutzeri* ZoBell, the *ccoM* gene is located far away from the two *cbb*$_3$ operons consisting of the structural genes (PstZoBell_18660 to PstZoBell_19488) that encode the two isoforms of Cbb_3-C*c*O. We found that the genes coding for a DNA repair system protein (PstZoBell_05026) and a type II secretory pathway protein (PstZoBell_05041) are located immediately upstream and downstream of *ccoM*, respectively (Fig. 3A). Promoter prediction indicated that a putative promoter is present upstream of *ccoM* (Fig. 3B). A putative arginine nitrate regulator

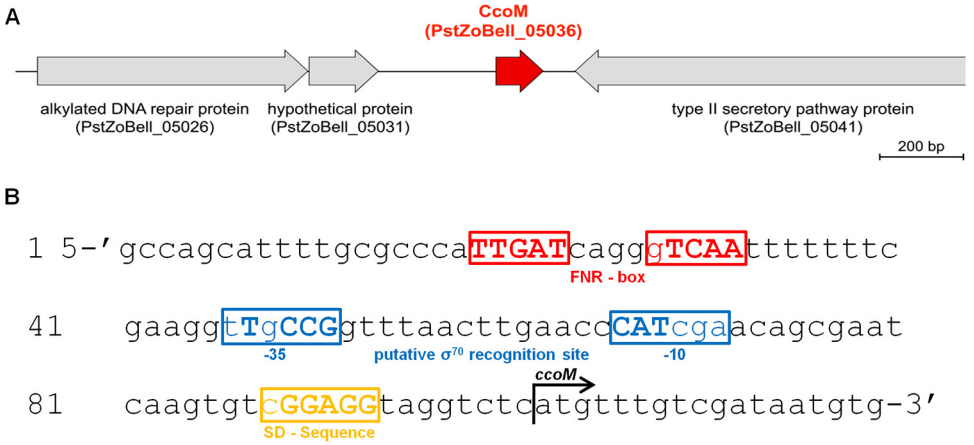

FIG 3 Location and upstream region of the *ccoM* gene. (A) Location of *ccoM* in *P. stutzeri* ZoBell genome. The *ccoM* gene (locus tag, PstZoBell_05036) is shown in red. Genes encoding an alkylated DNA repair protein (PstZoBell_05026), hypothetical protein (PstZoBell_05031), and type II secretory pathway protein (PstZoBell_05041) are shown in grey; PstZoBell_05026 and PstZoBell_05031 are positioned upstream of *ccoM*, and PstZoBell_05041 is positioned downstream. (B) Nucleotide sequence (5′ to 3′) of the *ccoM* upstream region. Sequences in the red boxes exhibit homology to an ANR (FNR) box (TTGAT-N4-gTCAA). Based on the data from *P. putida* (48), a putative σ^{70}-containing RNA polymerase recognition site with the −35 and −10 regions is shown in blue. A potential Shine-Dalgarno (SD) sequence located upstream of the *ccoM* transcription start site is indicated in orange. The consensus sequences are capitalized. The *ccoM* translation initiation site is indicated by a black arrow.

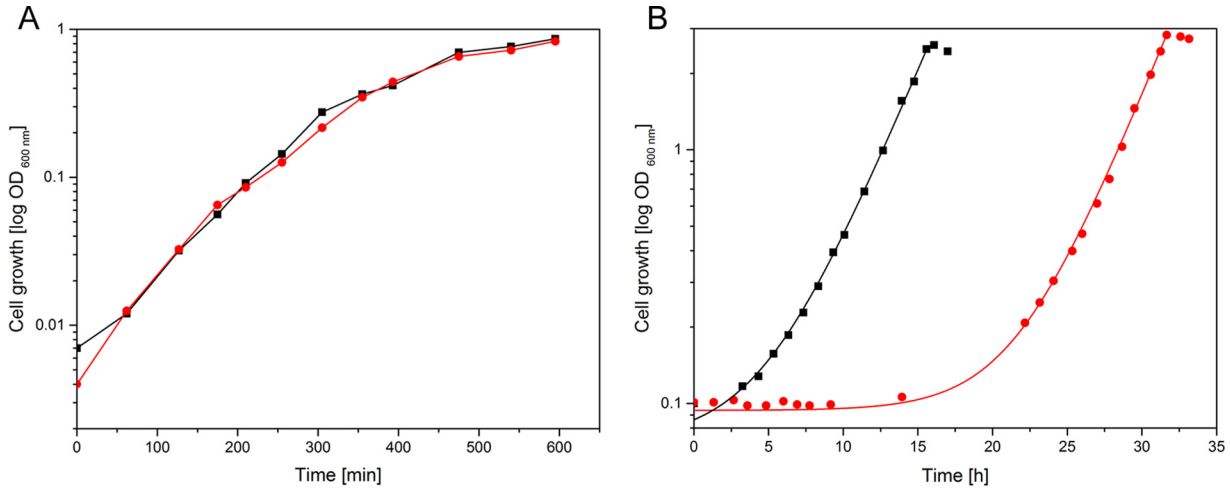

FIG 4 Cell growth of wild-type (black line) and ΔCcoM (red line) *P. stutzeri* ZoBell strains. (A) Microaerobic growth conditions. (B) Anaerobic denitrifying growth conditions. The data points of both growth curves were fitted exponentially until the stationary phase is reached.

(ANR) binding motif, homologous to the *Escherichia coli* fumarate and nitrate reduction regulator (FNR) motif, is found in the predicted promoter of *ccoM* (TTGAT-N4-gTCAA) (Fig. 3B). An ANR box is also present in the upstream region of *ccoN*-1 (17) and indicates a simultaneous upregulation of *ccoM* and cbb_3-1 under conditions of low oxygen concentrations (18, 19). Furthermore, an NCBI BLAST search for the CcoM protein sequences in the complete proteome database showed that this protein is almost exclusively present in species of the genus *Pseudomonas*. The CcoM homologues have similar lengths (35 to 39 amino acids). Several key residues of CcoM that contribute to the proposed interaction with CcoN (M17, F20, and F24 [*P. stutzeri* ZoBell CcoM numbering]) are highly conserved in CcoM homologues. Residues M17 and F20 are conserved in all indicated CcoM homologues, whereas F24 is sometimes replaced by valine or leucine (see Table S4 in the supplemental material). In other pseudomonads, the localization of this gene is similar to that of the *ccoM* gene in *P. stutzeri*. However, these CcoM-related proteins are partially annotated as ATP-dependent helicases, probably due to their genomic location (see Table S4).

Functional characterization of ΔCcoM strain. In order to characterize the physiological function of CcoM in the Cbb_3-C*c*O complex, we created a knockout strain (ΔCcoM variant) of *P. stutzeri* ZoBell. To confirm the absence of CcoM in Cbb_3-1, MALDI-TOF MS measurements of the purified Cbb_3-1–ΔCcoM variant were performed. As expected, the spectrum does not show any peak in the range from 2 to 15 kDa (see Fig. S3 in the supplemental material).

We subsequently tested bacterial cell growth under different conditions; the wild-type strain and the ΔCcoM strain did not show any observable differences concerning their growth behavior under microaerobic conditions (Fig. 4A). Under anaerobic denitrifying conditions, however, we observed a significant increase in the lag phase of the ΔCcoM *P. stutzeri* strain compared to the wild-type strain (Fig. 4B). The cultures were inoculated to an optical density at 600 nm (OD_{600}) of 0.1, and the cells of the ΔCcoM *P. stutzeri* strain reached an OD_{600} of 0.3 after 25 h ± 1 h, whereas the wild-type cells already showed an OD_{600} of 0.3 after 10.1 h ± 1.7 h. However, in the log phase, the cells of the two strains had similar doubling times of 193 min ± 46 min (wild-type strain) and 201 min ± 24 min (ΔCcoM strain).

In addition, to gain insights into the significance of both cbb_3 isoforms under different conditions, we compared the growth behaviors of the ΔCbb_3-1 and ΔCbb_3-2 *P. stutzeri* deletion strains to that of the wild-type strain (see Fig. S4 in the supplemental material). Under microaerobic conditions, the growth of the ΔCbb_3-2 strain was slightly delayed compared to growth of the wild-type and ΔCbb_3-1 strains, since the Cbb3-2 is particularly important under aerobic conditions which are present at the beginning of the cell growth. We observed that, under anaerobic denitrifying conditions, the ΔCbb_3-1 cells had already grown to an OD_{600} of 0.3 after 5.2 h ± 0.18 h, whereas the ΔCbb_3-2 cells had reached an OD_{600} of 0.3 only after 14.7 h ± 1.1 h. (versus an OD_{600} of 0.3 after 10.1 h ± 1.7 h for wild-type *P. stutzeri*).

The purified wild-type Cbb_3-1 and Cbb_3-1–ΔCcoM oxidases were compared using UV-vis spectroscopy, differential scanning calorimetry (DSC), and oxygen reductase activity measurements.

We used UV-vis spectroscopy to characterize the hemes in cbb_3-C*c*O. The states of the *b*- and *c*-type hemes can be analyzed using the absorption maxima at 411 nm (Soret band), 552 nm (α-band), and 522 nm (β-band) as well as the shoulders at 559 and 529 nm (Fig. 5A). We conclude from the identical Cbb_3-1 and Cbb_3-1–ΔCcoM spectra that there were no differences concerning heme incorporation and heme environments.

DSC was conducted to compare the stabilities of the recombinant (rec.) Cbb_3-1 and rec. Cbb_3-1–ΔCcoM variants by monitoring the melting temperature (T_m) profiles (Fig. 5B). Peaks 1 and 2 correspond to the denaturation of the Cbb_3 complex. The shifts in the T_m values of peaks 1 and 2 between the wild type and the Cbb_3-1–ΔCcoM variant indicate a decreased thermal stability of the Cbb_3-1–ΔCcoM variant compared to the wild type. An identical trend was observed after 16 days, with the deletion variant displaying lower melting temperatures similar to those seen with the wild type (data not shown).

We determined the oxygen consumption rates of *P. stutzeri* membranes prepared from wild-type and ΔCcoM cells as well as the oxygen reductase activities of purified wild-type Cbb_3-1 and the Cbb_3-1–ΔCcoM variant. The measurements were performed

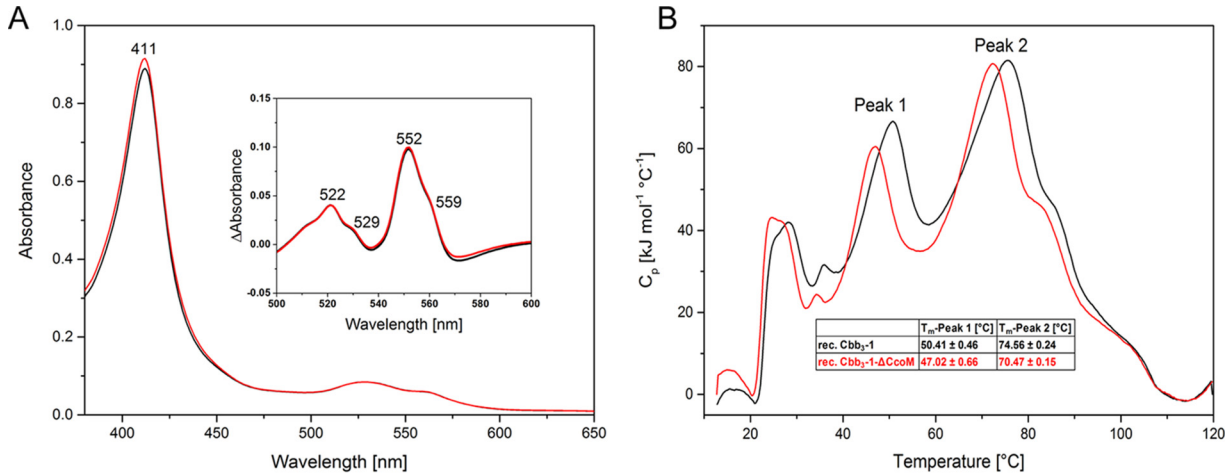

FIG 5 Characterization of the ΔCcoM variant. (A) UV-vis spectra of oxidized wild-type Cbb_3-1 (black line) and the Cbb_3-1–ΔCcoM variant (red line) at 380 to 650 nm with the Soret maxima at 411 nm. The inset shows the 500-to-600-nm region of the reduced-minus-oxidized difference spectra with the maxima (shoulders) of the α- and β-bands at 552 nm (559 nm) and 522 nm (529 nm), respectively. (B) DSC measurement of rec. wild-type Cbb_3-1 (black line) and the rec. Cbb_3-1–ΔCcoM variant (red line) at 10 to 120°C. The inset table indicates the T_m values of peak 1 and peak 2 with the errors determined from four measurements. The additional peak at T_m ~25 to ~30°C is caused by the presence of the detergent (61).

with an artificial electron donor system consisting of sodium-ascorbate and TMPD (N,N,N′,N′-tetramethyl-*p*-phenylenediamine dihydrochloride) under optimized conditions (17). We did not observe significant differences between wild-type and ΔCcoM membranes in the oxygen consumption rates. In addition, the purified Cbb_3-1–ΔCcoM variant had a catalytic activity of approximately 1,000 e^-/s and thus displayed wild-type-like activity (see Fig. S5 in the supplemental material).

DISCUSSION

Small subunits in membrane protein complexes. In this work, the CcoM subunit was identified as part of the cbb_3-C*c*O complex from *P. stutzeri* ZoBell after the crystallographic electron density map had indicated the presence of a fourth subunit. The situation resembles that of the aa_3-C*c*O of *Paracoccus denitrificans*, where the small subunit IV also was identified after an X-ray crystallographic structure determination (20). For the cbb_3-C*c*O from *P. stutzeri*, our DSC data indicate reduced thermal stability of the purified CcoM-deficient variant (Cbb_3-1–ΔCcoM) compared to the wild type, suggesting that CcoM is probably involved in complex stability and/or assembly. The presence of small subunits that are essential for assembly, stability, and activity is a common feature of membrane protein complexes (21–24). For instance, the ba_3-C*c*Os from *Thermus thermophilus* and *Aquifex aeolicus* contain one membrane-spanning helix, called subunit IIa (5, 25). Prunetti and coworkers proposed that subunit IIa is involved in the stability and/or assembly of ba_3-C*c*O (25). Furthermore, the small protein CydX was found to be a substantial part of the *bd*-oxidase complex in *Brucella abortus* and *E. coli*, as it is essential for enzymatic catalytic activity (26–28). It was shown for the cbb_3-C*c*O from *Rhodobacter capsulatus* that CcoH stably associates with the cbb_3 complex and constitutes an assembly factor (29, 30). Beyond enzymes of the superfamily of HCOs, small transmembrane-spanning subunits were also identified as part of bc_1 complexes and NAD(P)H dehydrogenases, for instance (31–34).

Comparison of CcoQ and CcoM. In *P. stutzeri* ZoBell, the *ccoQ* gene is present only in the operon encoding Cbb_3-2. Similarly to CcoM, CcoQ has one predicted TMH. The function of this subunit is still under debate (35–37). We set out to investigate whether CcoM is present also in Cbb_3-2 in addition to CcoQ. The results of our MALDI-TOF MS measurements suggest that CcoM indeed interacts with Cbb_3-2 (data not shown). However, it remains unclear if CcoM and CcoQ are located at identical or different positions in Cbb_3-2. Theoretically, CcoM and CcoQ may be functionally redundant due to their secondary structure resemblances. Using multiple sequence alignments of CcoQ subunits from different γ-proteobacteria and CcoM from *P. stutzeri* (Fig. 6), we found that CcoQ and CcoM share several highly conserved residues (G10, T13, M17-F20, and W29 [CcoM numbering]) in the N-terminal region. Furthermore, the conserved $M17^M$ and $F20^M$ amino acids are part of the proposed interaction ladder with CcoN. In CcoQ, residue $M17^M$ is replaced either by a phenylalanine (*Vibrio cholerae*) or by smaller hydrophobic residues like leucine (*Azotobacter vinelandii*) and valine (*P. stutzeri*). We are currently investigating the physiological roles of CcoM and CcoQ to determine if the two subunits perform distinct or similar functions.

Anaerobic growth of wild-type and *P. stutzeri* deletion strains under denitrifying conditions. In many pseudomonads, e.g., *Pseudomonas aeruginosa*, *P. stutzeri*, and *P. putida*, two cbb_3 operons are present in the genome (8, 17, 38). However, only one of the two operons is preceded by an ANR box in its promoter region. In *P. aeruginosa*, the expression of the ANR-dependent cbb_3 isoform is highly upregulated under low-oxygen conditions and in the stationary phase. In contrast, the ANR-independent one is constitutively expressed and not directly dependent on oxygen concentrations (8, 39). Recently, Hamada and coworkers showed that the *P. aeruginosa* cbb_3-C*c*Os accumulate nitric oxide and are involved in biofilm formation during the anaerobic denitrification process (40). In addition, cbb_3-C*c*Os were reported to be expressed under anaerobic conditions in several other bacterial species, e.g., *Shewanella oneidensis*, *Bradyrhizobium japonicum*, and *Rhodobacter capsulatus* (19, 41, 42). In this work, the growth behaviors of wild-type, ΔCbb_3-1, ΔCbb_3-2, and ΔCcoM *P. stutzeri*

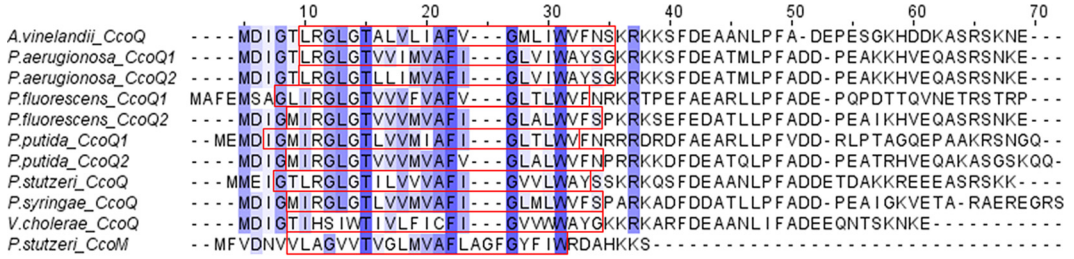

FIG 6 Multiple sequence alignment of subunit CcoM from *P. stutzeri* and CcoQ subunits from γ-proteobacteria. Red boxes indicate the predicted TMH region. The intensity of the blue coloring of amino acids reflects the degree of conservation. Multiple sequence alignment was performed with Jalview (62). CcoQ and CcoM sequences from *A. vinelandii* DJ (GenBank accession no. YP_002799181.1), *P. aeruginosa* PAO1 (GenBank accession no. YP_003933610.1, YP_003933611.1), *P. fluorescens* Pf0-1 (GenBank accession no. YP_347557.1 and YP_347553.1), *P. putida* KT2440 (GenBank accession no. NP_746368.1 and NP_746373.1), *P. stutzeri* ZoBell (accession no. ADJ00005.1 and EHY76787.1), *P. syringae* B728a (GenBank accession no. YP_236485.1), and *V. cholerae* O1 N16961 (GenBank accession no. NP_231083.1) strains were aligned.

ZoBell strains were studied anaerobically under denitrifying conditions (Fig. 4B; see also Fig. S4B in the supplemental material). Compared to the wild type, the ΔCbb_3-1 strain is characterized by a shortened lag phase. Results of previous studies on *Rhodobacter sphaeroides* suggest that the electron flow through *cbb*$_3$-C*c*O is inversely related to the level of expression of photosynthetic genes through the PrrBA two-component regulatory system (43–45). The PrrBA system is also involved in the regulation of the denitrification pathway and is an analog to the RoxSR system of *Pseudomonas* (46–48). The absence of Cbb_3-1 in the ΔCbb_3-1 *P. stutzeri* cells might have led to the loss of the inhibitory signal that potentially represses denitrification gene expression. As a consequence, an increased expression level of denitrification enzymes may explain why the growth of ΔCbb_3-1 during the lag phase is faster than that of the wild-type *P. stutzeri* strain. In contrast to the ΔCbb_3-1 results, we observed an extended lag phase of the ΔCbb_3-2 strain compared to the wild type. However, the role of Cbb_3-2 under anaerobic denitrifying conditions remains to be elucidated. Similarly to Cbb_3-1, the promoter region of CcoM also contains an ANR box, indicating its significance under low-oxygen conditions. Beyond its functions as a bona fide subunit of *cbb*$_3$-C*c*O, the extended lag phase of the ΔCcoM strain under anaerobic denitrifying conditions also suggests that CcoM may interact with proteins involved in the denitrification process. Further investigations, e.g., *in vivo* cross-linking experiments and whole-proteome studies of the CcoM deletion strain under anaerobic conditions, are required to analyze the physiological role of CcoM in more detail.

In summary, we unambiguously identified the uncharacterized TMH in the Cbb_3 crystal structure by MALDI-TOF MS/MS as PstZoBell_05036. The gene encoding this protein is located outside the *cbb*$_3$ operon and was renamed *ccoM*. We fitted the CcoM sequence into the unknown TMH of the X-ray structure, successfully matching bulky amino acid side chains to the observed electron densities. In the structure, CcoM interacts with two helices of the catalytic subunit CcoN in a ladder-like conformation. Taken together, these data indicate that we have indeed identified the unknown subunit. Previously, this subunit had been assigned to the *cbb*$_3$-C*c*O biogenesis protein CcoH (49). The assumption was based on the observation that CcoH can be found as a minor contaminant in the purified *cbb*$_3$ isoforms (17) and CcoH's secondary structure and on CcoH's importance for the *cbb*$_3$-C*c*O function (50). The mode of interaction of CcoM with subunit CcoN also appears to be exclude the possibility that this subunit contributes to a transient proton-conducting network. While we observed no effect on heme incorporation and catalytic activity, the C*c*O complex lacking CcoM displayed significantly reduced melting temperatures in DSC, suggesting a putative role of CcoM in complex assembly and stability.

MATERIALS AND METHODS

Bacterial strains, media, and oligonucleotides. *Pseudomonas stutzeri* strain ZoBell (ATCC 14405) was used to construct a deletion strain of the *ccoM* gene (locus tag, PstZoBell_05036), resulting in the Δ*ccoM* strain. The *P. stutzeri* ZoBell cells were grown on lysogeny broth (LB) agar plates and in asparagine minimal medium at 32°C (10, 11). Antibiotics were added to final concentrations of 100 μg/ml kanamycin and 170 μg/ml chloramphenicol. *Escherichia coli* strain DH5α was used for cloning purposes (51). DNA sequencing was performed by Eurofins MWG Operon (Ebersberg, Germany). Plasmids and synthetic oligonucleotides (Eurofins MWG Operon) prepared for this study are listed in Tables S1 and S2 in the supplemental material, respectively.

Construction of Δ*ccoM P. stutzeri* strain. The lambda Red recombinase system (52) was used to replace *ccoM* (PstZoBell_05036) in the *P. stutzeri* ZoBell genome by a kanamycin resistance cassette. To construct a helper plasmid for the homologous recombination, genes *araC*, *gam*, *bet*, and *exo* were amplified from the pUCP18-RedS vector (53) into the linearized pBBR1MCS (54) vector, employing ligation-independent cloning techniques (In-Fusion cloning kit; Clontech, Mountain View, CA). The resulting pMK-RedS vector was electrotransformed into *P. stutzeri* ZoBell cells (55). The *P. stutzeri* ZoBell cells containing pMK-RedS were cultured in LB media at 32°C and 180 rpm to an optical density at 600 nm (OD_{600}) of 0.5 to 0.6. Expression of proteins Gam, Bet, and Exo was then induced with 0.2% (wt/vol) L-arabinose. After 4 h of induction, the *P. stutzeri* ZoBell cells were electrotransformed with approximately 5 μg of linearized DNA and incubated in super-optimal-broth (SOC) medium without antibiotics at 37°C with shaking (180 rpm) for 2 h. The linearized DNA was generated by 3-step PCR as previously described (56) and contained a kanamycin resistance cassette with long (~500-bp) flanking regions upstream and downstream of the *ccoM* gene. The gene disruption was confirmed by kanamycin resistance selection, PCR, and sequencing (Eurofins MWG Operon, Ebersburg, Germany) (see Fig. S1 in the supplemental material). Curing of the pMK-RedS plasmid from the deletion strain was carried out using electroporation (57).

Cultivations of *P. stutzeri* and purification of Cbb_3-C*c*O. *P. stutzeri* ZoBell cells were cultured under microaerobic conditions and harvested as previously published (10). All cultivations were perform in L-asparagine minimal media (10, 11), unless stated otherwise. For anaerobic cultivation under denitrifying conditions, *P. stutzeri* was grown in L-asparagine minimal media with 11.8 mM KNO_3 at 32°C and 260 rpm in a 2-liter fermenter with continuously injection of nitrogen. KNO_3 (11.8 mM) was additionally supplemented at OD_{600} values of 0.3 and 0.7.

Membrane preparation and solubilization were performed according to previously described procedures with cells grown under microaerobic conditions (10, 11). Genomically expressed Cbb_3-1 was purified from membranes prepared from the wild-type and ΔCcoM *P. stutzeri* strains, yielding wild-type Cbb_3-1 and Cbb_3-1–ΔCcoM, respectively. The four-step chromatographic purification of both enzymes was carried as published previously (11), and both purified enzymes were analyzed using UV-vis spectroscopy and oxygen reductase activity measurements. For differential scanning calorimetry (DSC) measurements, plasmid-expressed recombinant Cbb_3-1 was produced using expression vector pXH-22 (17) in the wild-type strain and the ΔCcoM strain. The purification of this streptavidin (Strep)-tagged recombinant Cbb_3-1 was performed as previously described (17).

Purification and sequencing of CcoM (mass spectrometry). CcoM was purified from Cbb_3-C*c*O using c4-ZipTips (Merck, Germany). The peptides were eluted in gradients of acetonitrile (30%, 50%, and 90% [vol/vol] acetonitrile–water–0.1% [vol/vol] trifluoroacetic acid [TFA]). The 90% acetonitrile elution fraction was lyophilized and redissolved in 20 μl of 90% (vol/vol) acetonitrile–10% (vol/vol) water–0.1% (vol/vol) TFA. A MALDI matrix solution was generated from 50 mg SDHB (Bruker, Germany) (9:1 mixture of 2,5-dihydroxybenzoic acid and 2-methoxy-5-hydroxybenzoic acid) dissolved in 1 ml 50% (vol/vol) acetonitrile–50% (vol/vol) water–0.1% (vol/vol) TFA. An aliquot of the fraction was then mixed 1:1 with matrix solution, and portions of 1 μl were deposited on a stainless steel target and dried in ambient air. MS and MS/MS spectra were acquired using an ultrafleXtreme (Bruker, Germany) in positive-ion mode. Compass 1.4 (Bruker, Germany) was used for acquisition and processing of spectra, and Mascot 2.4 (Matrixscience, United Kingdom) and BioTools 3.2 (Bruker, Germany) were used for database searches and interpretation of spectra. In the first step of data interpretation, sequence tags were generated *de novo* for protein identification using MS-BLAST 2.0 at Harvard Medical School (58).

Structure refinement. Residues 1 to 29 of PstZoBell_05036 were fitted into the electron density map of the unknown transmembrane helix in the electron density map of the Cbb_3-1 cytochrome *c* oxidase (PDB ID: 3MK7) using COOT (59). Refinement performed with Phenix (60) resulted in an R/R_{free} value of 18.7/22.3% and a root mean square (RMS) deviation for bond lengths of 0.009 Å in the resolution range 15.0 to 3.2 Å.

UV-vis spectrophotometry. UV-vis spectra of Cbb_3-C*c*O were recorded with a Lambda 35 UV-vis spectrophotometer (PerkinElmer, Waltham, MA) at a wavelength range of 380 to 650 nm. Purified Cbb_3-C*c*O (1 to 2 μM) was oxidized in a reaction mixture containing 20 mM Tris-HCl (pH 7.5), 100 mM NaCl, 50 μM EDTA, 10% (vol/vol) glycerol, and 0.02% (wt/vol) DDM (n-dodecyl-β-D-maltoside) (Cbb_3 buffer) with an excess of potassium hexacyanoferrate (III) and reduced by adding small amounts of solid sodium dithionite.

Differential scanning calorimetry. Differential scanning calorimetry (DSC) was used to compare the melting temperatures (T_m) of recombinant wild-type Cbb_3-1 and the recombinant Cbb_3-1–ΔCcoM variant. In order to obtain DSC data with a sufficient signal-to-noise ratio, the measurements were performed with a Cbb_3-C*c*O concentration of 5 mg/ml. The DSC measurements were performed using a Microcal VP-DSC capillary cell microcalorimeter (Malvern Instruments, Worchestershire, United Kingdom). Scans were carried out with rec. Cbb_3-C*c*O in Cbb_3 buffer in a temperature range of 10 to 120°C with a scan rate of 90°C/h and a 10-s filtering period in the low-feedback mode. Data analyses were done with origin 8.6 (Additive GmbH, Friedrichsdorf, Germany).

Oxygen reductase activity measurements. The oxygen consumption rates of *P. stutzeri* membranes and of purified Cbb_3-C*c*O were determined using polarography performed with a Clark-type oxygen electrode linked to a PA 2000 picoammeter (Unisense, Aarhus, Denmark) (both OX-MR). The signals were converted from analog to digital data using an A/D converter (ADC-216; Unisense) and recorded with the manufacturer's SensorTrace Basic 2.1 software. During the measurement, the samples were stirred in a 2-ml glass vial with a reaction volume of 600 μl in a water bath at room temperature. The oxygen consumption was initiated by adding 4 to 50 μg homogenized (or solubilized) membrane proteins or by adding 8.3 nM purified Cbb_3-C*c*O, respectively, to the buffer (50 mM Tris-HCl [pH 7.5], 100 mM NaCl with or without 0.02% [wt/vol] DDM) containing 3 mM sodium-ascorbate and 1 mM TMPD (N,N,N′,N′-tetramethyl-*p*-phenylenediamine dihydrochloride) (17). Data were analyzed with origin 8.6 (Additive GmbH, Friedrichsdorf, Germany).

Protein structure accession number. The updated X-ray structure of the Cbb_3-1 cytochrome *c* oxidase was deposited in the Protein Data Bank (PDB file 5DJQ).

SUPPLEMENTAL MATERIAL

Supplemental material for this article may be found at http://mbio.asm.org/lookup/suppl/doi:10.1128/mBio.01921-15/-/DCSupplemental.

Figure S1, TIF file, 0.3 MB.
Figure S2, TIF file, 2 MB.
Figure S3, TIF file, 0.1 MB.
Figure S4, TIF file, 0.5 MB.
Figure S5, TIF file, 0.6 MB.
Table S1, PDF file, 0.2 MB.
Table S2, PDF file, 0.1 MB.
Table S3, PDF file, 0.1 MB.
Table S4, PDF file, 0.03 MB.

ACKNOWLEDGMENTS

We thank Imke Wüllenweber, Fiona Rupprecht, Hannelore Müller, and Cornelia Münke for excellent technical assistance. Ulrich Ermler and Florian Hilbers contributed with fruitful discussions. Furthermore, we thank Laurence Rahme (Harvard Medical School, Boston, MA, USA) for providing the vector pUCP18-RedS.

FUNDING INFORMATION

This work was financially supported by the Max Planck Society and the Deutsche Forschungsgemeinschaft (Cluster of Excellence Frankfurt, Macromolecular Complexes).

REFERENCES

1. **Murima P, McKinney JD, Pethe K.** 2014. Targeting bacterial central metabolism for drug development. Chem Biol **21:**1423–1432. http://dx.doi.org/10.1016/j.chembiol.2014.08.020.
2. **Castresana J, Saraste M.** 1995. Evolution of energetic metabolism: the respiration-early hypothesis. Trends Biochem Sci **20:**443–448. http://dx.doi.org/10.1016/S0968-0004(00)89098-2.
3. **Iwata S, Ostermeier C, Ludwig B, Michel H.** 1995. Structure at 2.8-A resolution of cytochrome *c* oxidase from Paracoccus denitrificans. Nature **376:**660–669. http://dx.doi.org/10.1038/376660a0.
4. **Lyons JA, Aragão D, Slattery O, Pisliakov AV, Soulimane T, Caffrey M.** 2012. Structural insights into electron transfer in caa3-type cytochrome oxidase. Nature **487:**514–518. http://dx.doi.org/10.1038/nature11182.
5. **Soulimane T, Than ME, Dewor M, Huber R, Buse G.** 2000. Primary structure of a novel subunit in ba3-cytochrome oxidase from Thermus thermophilus. Protein Sci **9:**2068–2073. http://dx.doi.org/10.1110/ps.9.11.2068.
6. **Buschmann S, Warkentin E, Xie H, Langer JD, Ermler U, Michel H.** 2010. The structure of cbb3 cytochrome oxidase provides insights into proton pumping. Science **329:**327–330. http://dx.doi.org/10.1126/science.1187303.
7. **Pitcher RS, Watmough NJ.** 2004. The bacterial cytochrome cbb3 oxidases. Biochim Biophys Acta **1655:**388–399. http://dx.doi.org/10.1016/j.bbabio.2003.09.017.
8. **Comolli JC, Donohue TJ.** 2004. Differences in two Pseudomonas aeruginosa cbb3 cytochrome oxidases. Mol Microbiol **51:**1193–1203. http://dx.doi.org/10.1046/j.1365-2958.2003.03904.x.
9. **Cosseau C, Batut J.** 2004. Genomics of the ccoNOQP-encoded cbb3 oxidase complex in bacteria. Arch Microbiol **181:**89–96. http://dx.doi.org/10.1007/s00203-003-0641-5.
10. **Urbani A, Gemeinhardt S, Warne A, Saraste M.** 2001. Properties of the detergent solubilised cytochrome *c* oxidase (cytochrome cbb(3)) purified

from Pseudomonas stutzeri. FEBS Lett **508:**29–35. http://dx.doi.org/10.1016/S0014-5793(01)03006-X.
11. **Buschmann S, Richers S, Ermler U, Michel H.** 2014. A decade of crystallization drops: crystallization of the cbb3 cytochrome *c* oxidase from Pseudomonas stutzeri. Protein Sci **23:**411–422. http://dx.doi.org/10.1002/pro.2423.
12. **Peña A, Busquets A, Gomila M, Bosch R, Nogales B, García-Valdés E, Lalucat J, Bennasar A.** 2012. Draft genome of Pseudomonas stutzeri strain zobell (CCUG 16156), a marine isolate and model organism for denitrification studies. J Bacteriol **194:**1277–1278. http://dx.doi.org/10.1128/JB.06648-11.
13. **Von Heijne G, Gavel Y.** 1988. Topogenic signals in integral membrane proteins. Eur J Biochem **174:**671–678. http://dx.doi.org/10.1111/j.1432-1033.1988.tb14150.x.
14. **Aravinda S, Shamala N, Das C, Sriranjini A, Karle IL, Balaram P.** 2003. Aromatic-aromatic interactions in crystal structures of helical peptide scaffolds containing projecting phenylalanine residues. J Am Chem Soc **125:**5308–5315. http://dx.doi.org/10.1021/ja0341283.
15. **Ringer AL, Senenko A, Sherrill CD.** 2007. Models of S/pi interactions in protein structures: comparison of the H2S benzene complex with PDB data. Protein Sci **16:**2216–2223. http://dx.doi.org/10.1110/ps.073002307.
16. **Ridder A, Skupjen P, Unterreitmeier S, Langosch D.** 2005. Tryptophan supports interaction of transmembrane helices. J Mol Biol **354:**894–902. http://dx.doi.org/10.1016/j.jmb.2005.09.084.
17. **Xie H, Buschmann S, Langer JD, Ludwig B, Michel H.** 2014. Biochemical and biophysical characterization of the two isoforms of cbb3-type cytochrome *c* oxidase from Pseudomonas stutzeri. J Bacteriol **196:**472–482. http://dx.doi.org/10.1128/JB.01072-13.
18. **Mouncey NJ, Kaplan S.** 1998. Oxygen regulation of the ccoN gene encoding a component of the cbb3 oxidase in Rhodobacter sphaeroides 2.4.1T: involvement of the FnrL protein. J Bacteriol **180:**2228–2231.
19. **Swem DL, Bauer CE.** 2002. Coordination of ubiquinol oxidase and cytochrome cbb(3) oxidase expression by multiple regulators in Rhodobacter capsulatus. J Bacteriol **184:**2815–2820. http://dx.doi.org/10.1128/JB.184.10.2815-2820.2002.
20. **Witt H, Ludwig B.** 1997. Isolation, analysis, and deletion of the gene coding for subunit IV of cytochrome *c* oxidase in Paracoccus denitrificans. J Biol Chem **272:**5514–5517. http://dx.doi.org/10.1074/jbc.272.9.5514.
21. **Zickermann V, Angerer H, Ding MG, Nübel E, Brandt U.** 2010. Small single transmembrane domain (STMD) proteins organize the hydrophobic subunits of large membrane protein complexes. FEBS Lett **584:**2516–2525. http://dx.doi.org/10.1016/j.febslet.2010.04.021.
22. **Shi LX, Schröder WP.** 2004. The low molecular mass subunits of the photosynthetic supracomplex, photosystem II. Biochim Biophys Acta **1608:**75–96. http://dx.doi.org/10.1016/j.bbabio.2003.12.004.
23. **Takahashi Y, Rahire M, Breyton C, Popot JL, Joliot P, Rochaix JD.** 1996. The chloroplast ycf7 (petL) open reading frame of Chlamydomonas reinhardtii encodes a small functionally important subunit of the cytochrome *b6*f complex. EMBO J **15:**3498–3506.
24. **Berthold DA, Schmidt CL, Malkin R.** 1995. The deletion of petG in Chlamydomonas reinhardtii disrupts the cytochrome bf complex. J Biol Chem **270:**29293–29298. http://dx.doi.org/10.1074/jbc.270.49.29293.
25. **Prunetti L, Brugna M, Lebrun R, Giudici-Orticoni MT, Guiral M.** 2011. The elusive third subunit IIa of the bacterial B-type oxidases: the enzyme from the hyperthermophile Aquifex aeolicus. PLoS One **6:**e21616. http://dx.doi.org/10.1371/journal.pone.0021616.
26. **Hoeser J, Hong S, Gehmann G, Gennis RB, Friedrich T.** 2014. Subunit CydX of Escherichia coli cytochrome *bd* ubiquinol oxidase is essential for assembly and stability of the di-heme active site. FEBS Lett **588:**1537–1541. http://dx.doi.org/10.1016/j.febslet.2014.03.036.
27. **VanOrsdel CE, Bhatt S, Allen RJ, Brenner EP, Hobson JJ, Jamil A, Haynes BM, Genson AM, Hemm MR.** 2013. The Escherichia coli CydX protein is a member of the CydAB cytochrome *bd* oxidase complex and is required for cytochrome *bd* oxidase activity. J Bacteriol **195:**3640–3650. http://dx.doi.org/10.1128/JB.00324-13.
28. **Sun YH, de Jong MF, den Hartigh AB, Roux CM, Rolán HG, Tsolis RM.** 2012. The small protein CydX is required for function of cytochrome *bd* oxidase in Brucella abortus. Front Cell Infect Microbiol **2:**47. http://dx.doi.org/10.3389/fcimb.2012.00047.
29. **Kulajta C, Thumfart JO, Haid S, Daldal F, Koch HG.** 2006. Multi-step assembly pathway of the cbb3-type cytochrome *c* oxidase complex. J Mol Biol **355:**989–1004. http://dx.doi.org/10.1016/j.jmb.2005.11.039.
30. **Pawlik G, Kulajta C, Sachelaru I, Schröder S, Waidner B, Hellwig P, Daldal F, Koch HG.** 2010. The putative assembly factor CcoH is stably associated with the cbb3-type cytochrome oxidase. J Bacteriol **192:**6378–6389. http://dx.doi.org/10.1128/JB.00988-10.
31. **Rodgers S, Moser C, Martinez-Julvez M, Sinning I.** 2000. Deletion of the 6-kDa subunit affects the activity and yield of the BC 1 complex from Rhodovulum sulfidophilum. Eur J Biochem **267:**3753–3761. http://dx.doi.org/10.1046/j.1432-1327.2000.01411.x.
32. **Nowaczyk MM, Wulfhorst H, Ryan CM, Souda P, Zhang H, Cramer WA, Whitelegge JP.** 2011. NdhP and NdhQ: two novel small subunits of the cyanobacterial NDH-1 complex. Biochemistry **50:**1121–1124. http://dx.doi.org/10.1021/bi102044b.
33. **Zhang J, Gao F, Zhao J, Ogawa T, Wang Q, Ma W.** 2014. NdhP is an exclusive subunit of large complex of NADPH dehydrogenase essential to stabilize the complex in Synechocystis sp. strain pcc 6803. J Biol Chem **289:**18770–18781. http://dx.doi.org/10.1074/jbc.M114.553404.
34. **Zhao J, Rong W, Gao F, Ogawa T, Ma W.** 2015. Subunit Q is required to stabilize the large complex of NADPH dehydrogenase in Synechocystis sp. Strain PCC 6803. Plant Physiol **168:**443–451. http://dx.doi.org/10.1104/pp.15.00503.
35. **Zufferey R, Preisig O, Hennecke H, Thöny-Meyer L.** 1996. Assembly and function of the cytochrome cbb3 oxidase subunits in Bradyrhizobium japonicum. J Biol Chem **271:**9114–9119. http://dx.doi.org/10.1074/jbc.271.15.9114.
36. **Peters A, Kulajta C, Pawlik G, Daldal F, Koch HG.** 2008. Stability of the cbb3-type cytochrome oxidase requires specific CcoQ-CcoP interactions. J Bacteriol **190:**5576–5586. http://dx.doi.org/10.1128/JB.00534-08.
37. **Oh JI, Kaplan S.** 2002. Oxygen adaptation. The role of the CcoQ subunit of the cbb3 cytochrome *c* oxidase of Rhodobacter sphaeroides 2.4.1. J Biol Chem **277:**16220–16228.
38. **Ugidos A, Morales G, Rial E, Williams HD, Rojo F.** 2008. The coordinate regulation of multiple terminal oxidases by the Pseudomonas putida ANR global regulator. Environ Microbiol **10:**1690–1702. http://dx.doi.org/10.1111/j.1462-2920.2008.01586.x.
39. **Kawakami T, Kuroki M, Ishii M, Igarashi Y, Arai H.** 2010. Differential expression of multiple terminal oxidases for aerobic respiration in Pseudomonas aeruginosa. Environ Microbiol **12:**1399–1412. http://dx.doi.org/10.1111/j.1462-2920.2009.02109.x.
40. **Hamada M, Toyofuku M, Miyano T, Nomura N.** 2014. cbb3-type cytochrome *c* oxidases, aerobic respiratory enzymes, impact the anaerobic life of Pseudomonas aeruginosa PAO1. J Bacteriol **196:**3881–3889. http://dx.doi.org/10.1128/JB.01978-14.
41. **Rosenbaum MA, Bar HY, Beg QK, Segrè D, Booth J, Cotta MA, Angenent LT.** 2012. Transcriptional analysis of Shewanella oneidensis MR-1 with an electrode compared to Fe(III)citrate or oxygen as terminal electron acceptor. PLoS One **7:**e30827. http://dx.doi.org/10.1371/journal.pone.0030827.
42. **Bueno E, Richardson DJ, Bedmar EJ, Delgado MJ.** 2009. Expression of Bradyrhizobium japonicum cbb(3) terminal oxidase under denitrifying conditions is subjected to redox control. FEMS Microbiol Lett **298:**20–28. http://dx.doi.org/10.1111/j.1574-6968.2009.01711.x.
43. **Kim YJ, Ko IJ, Lee JM, Kang HY, Kim YM, Kaplan S, Oh JI.** 2007. Dominant role of the cbb3 oxidase in regulation of photosynthesis gene expression through the PrrBA system in Rhodobacter sphaeroides 2.4.1. J Bacteriol **189:**5617–5625.
44. **Oh JI, Kaplan S.** 2000. Redox signaling: globalization of gene expression. EMBO J **19:**4237–4247. http://dx.doi.org/10.1093/emboj/19.16.4237.
45. **Oh JI, Ko IJ, Kaplan S.** 2004. Reconstitution of the Rhodobacter sphaeroides cbb3-PrrBA signal transduction pathway in vitro. Biochemistry **43:**7915–7923. http://dx.doi.org/10.1021/bi0496440.
46. **Carrica MDC, Fernandez I, Sieira R, Paris G, Goldbaum FA.** 2013. The two-component systems PrrBA and NtrYX co-ordinately regulate the adaptation of Brucella abortus to an oxygen-limited environment. Mol Microbiol **88:**222–233. http://dx.doi.org/10.1111/mmi.12181.
47. **Laratta WP, Choi PS, Tosques IE, Shapleigh JP.** 2002. Involvement of the PrrB/PrrA two-component system in nitrite respiration in Rhodobacter sphaeroides 2.4.3: evidence for transcriptional regulation. J Bacteriol **184:**3521–3529. http://dx.doi.org/10.1128/JB.184.13.3521-3529.2002.
48. **Arai H.** 2011. Regulation and function of versatile aerobic and anaerobic respiratory metabolism in Pseudomonas aeruginosa. Front Microbiol **2:**103. http://dx.doi.org/10.3389/fmicb.2011.00103.
49. **Muntyan MS, Cherepanov DA, Malinen AM, Bloch DA, Sorokin DY, Severina II, Ivashina TV, Lahti R, Muyzer G, Skulachev VP.** 2015. Cytochrome cbb3 of Thioalkalivibrio is a Na+-pumping cytochrome ox-

idase. Proc Natl Acad Sci U S A **112:**7695–7700. http://dx.doi.org/10.1073/pnas.1417071112.

50. **Ekici S, Pawlik G, Lohmeyer E, Koch HG, Daldal F.** 2012. Biogenesis of cbb(3)-type cytochrome *c* oxidase in Rhodobacter capsulatus. Biochim Biophys Acta **1817:**898–910. http://dx.doi.org/10.1016/j.bbabio.2011.10.011.
51. **Hanahan D.** 1983. Studies on transformation of Escherichia coli with plasmids. J Mol Biol **166:**557–580. http://dx.doi.org/10.1016/S0022-2836(83)80284-8.
52. **Shulman MJ, Hallick LM, Echols H, Signer ER.** 1970. Properties of recombination-deficient mutants of bacteriophage lambda. J Mol Biol **52:**501–520. http://dx.doi.org/10.1016/0022-2836(70)90416-X.
53. **Lesic B, Rahme LG.** 2008. Use of the lambda red recombinase system to rapidly generate mutants in Pseudomonas aeruginosa. BMC Mol Biol **9:**20. http://dx.doi.org/10.1186/1471-2199-9-20.
54. **Kovach ME, Phillips RW, Elzer PH, Roop RM, II, Peterson KM.** 1994. pBBR1MCS: a broad-host-range cloning vector. BioTechniques **16:**800–802.
55. **Choi KH, Kumar A, Schweizer HP.** 2006. A 10-min method for preparation of highly electrocompetent Pseudomonas aeruginosa cells: application for DNA fragment transfer between chromosomes and plasmid transformation. J Microbiol Methods **64:**391–397. http://dx.doi.org/10.1016/j.mimet.2005.06.001.
56. **Derbise A, Lesic B, Dacheux D, Ghigo JM, Carniel E.** 2003. A rapid and simple method for inactivating chromosomal genes in Yersinia. FEMS Immunol Med Microbiol **38:**113–116. http://dx.doi.org/10.1016/S0928-8244(03)00181-0.
57. **Heery DM, Powell R, Gannon F, Dunican LK.** 1989. Curing of a plasmid from E.coli using high-voltage electroporation. Nucleic Acids Res **17:**10131. http://dx.doi.org/10.1093/nar/17.23.10131.
58. **Shevchenko A, Sunyaev S, Loboda A, Shevchenko A, Bork P, Ens W, Standing KG.** 2001. Charting the proteomes of organisms with unsequenced genomes by MALDI-quadrupole time-of-flight mass spectrometry and BLAST homology searching. Anal Chem **73:**1917–1926. http://dx.doi.org/10.1021/ac0013709.
59. **Emsley P, Cowtan K.** 2004. Coot: model-building tools for molecular graphics. Acta Crystallogr D Biol Crystallogr **60:**2126–2132. http://dx.doi.org/10.1107/S0907444904019158.
60. **Adams PD, Grosse-Kunstleve RW, Hung LW, Ioerger TR, McCoy AJ, Moriarty NW, Read RJ, Sacchettini JC, Sauter NK, Terwilliger TC.** 2002. PHENIX: building new software for automated crystallographic structure determination. Acta Crystallogr D Biol Crystallogr **58:**1948–1954. http://dx.doi.org/10.1107/S0907444902016657.
61. **Hilbers F, von der Hocht I, Ludwig B, Michel H.** 2013. True wild type and recombinant wild type cytochrome *c* oxidase from Paracoccus denitrificans show a 20-fold difference in their catalase activity. Biochim Biophys Acta **1827:**319–327. http://dx.doi.org/10.1016/j.bbabio.2012.10.008.
62. **Waterhouse AM, Procter JB, Martin DM, Clamp M, Barton GJ.** 2009. Jalview version 2—a multiple sequence alignment editor and analysis workbench. Bioinformatics **25:**1189–1191. http://dx.doi.org/10.1093/bioinformatics/btp033.